LONGITUDINAL SPACE CHARGE EFFECTS IN RF BUCKETS*

W. S. Trzeciak
Midwestern Universities Research Association
Stoughton, Wisconsin

Summary

Longitudinal space charge effects in RF buckets have been studied by means of an IBM 704 computer program. This program simulates the motion of the particles in a beam under the influences of space charge forces and RF fields. Initially, the beam is given a small perturbation to excite a particular mode. Stable and unstable beams with energy spreads much greater than, approximately equal to, and much less than the energy spread of an RF bucket in the absence of space charge forces have been studied. Duplicate runs are made with and without space charge forces and the results are compared. After a transitional period of time, with space charge forces acting, the stable phase region assumes a characteristic diamond shape which persists for more than five synchrotron periods. This stable phase region contains more particles than the corresponding RF bucket in the absence of space charge forces. When the initial distribution of particles in phase space is independent of phase angle and has an energy spread much less than the energy spread necessary to stabilize the beam against the "negative mass" instability, large clumps of particles form immediately. These clumps of particles execute phase oscillations and may coagulate with the particles in the stable phase region. If particles far from the stable phase region do not interact with particles in the stable phase region, the bucket assumes an elliptical shape, very narrow in phase angle, large in energy spread, with a lifetime of more than five synchrotron periods.

Introduction

Theoretical analyses of longitudinal instabilities in coasting beams invariably involve differential equations for which exact, nontrivial solutions cannot easily be found. Solutions to the linearized equations[1, 2] have been accepted and shown to be good approximations. This approach fails to yield answers to two important questions: (1) How does a coasting beam develop when beam perturbations are no longer "small", and (2) How is the answer to the first question changed by the presence of RF fields?

*Work performed under the auspices of the U. S. Atomic Energy Commission.

The first question has been extensively studied by means of computer experiments.[2] Briefly, Dory's results indicate that any evenly distributed coasting beam above transition whose initial energy spread is one-half the "negative mass" instability limit, as given by Nielsen et al.,[1] immediately forms large clumps of particles which are very stable and which have a new energy spread given by (to 25 percent):

$$\Delta E_F = \frac{(\Delta E_{NM})^2}{\Delta E_I}$$

where: ΔE_F is the final energy spread, ΔE_I is the initial energy spread, and ΔE_{NM} is the energy spread just necessary to stabilize the beam. In the worst case, for a monoenergetic beam, Dory found that the final energy spread is never more than three times the stable energy spread.

This paper is concerned with a qualitative answer to the second question. Part I gives a brief development of the theory leading to the working equations of the computer program. Dory's technique (and computer program with minor changes)[2, 3] was used to study RF capture of initially stable and unstable coasting beams. Essentially this IBM 704 computer program computes the change in position and momentum of a large number of particles due to the space charge forces and RF fields. The space charge electric field is computed from the particle configuration at the previous time step. The particles are then moved in accordance with the changes in momentum and position. The resulting new particle configuration is used to determine the space charge field for the next time step. The total field acting on the particles is taken as the sum of an RF field term and the space charge electric field. In this way the particle motion can be monitored for long periods of time, far into the nonlinear region.

The computer experiments that were performed are presented in Part II. The form of the initial particle distributions is given. Pictorial results of some of the characteristic runs are presented. These results are mainly phase plots of the particles taken directly from the computer program output. A table of the results from all the experimental runs is given. The computer results show that the space charge forces tend to compress more particles into the

RF stable phase region if the initial energy spread is stable. Under similar conditions initially unstable beams lead to no stable phase motion.

I

The Hamiltonian* for a single particle subject to space charge forces as given by Nielsen and Sessler[4] is

$$H(W,\phi) = \pi h f_s f_s' W^2 + eV(t)\cos\phi + \dot{w}_s \phi - 2\pi eh\, U(\phi, t) \quad (1)$$

with the following usual definitions:
W, ϕ are canonical variables; $W \equiv w - w_s$ and $w \equiv \int_{E_o}^{E} \frac{dE'}{f(E')}$; and $\phi = h\theta$ in a coordinate system at rest relative to a synchronous particle. θ is the aximuth of a particle in the laboratory system (positive in the direction of particle revolution); h is the harmonic number; f_s is the frequency of a synchronous particle; f_s' is the rate of change of the frequency of a synchronous particle with respect to its energy; V(t) is the amplitude of the applied RF voltage; e is the electronic charge; and $U(\phi, t)$ is the space charge potential. The equations of motion are

$$\frac{d\phi}{dt} = \frac{\partial H}{\partial W} = 2\pi h f_s f_s' W \quad (2)$$

and

$$\frac{dW}{dt} = -\frac{\partial H}{\partial \phi} = -eV\left[\frac{\dot{w}_s}{eV} - \sin\phi\right] - 2\pi eR\,\mathcal{E}(\phi, t) \quad (3)$$

with

$$\mathcal{E}(\phi, t) = -\frac{h}{R}\frac{\partial U(\phi, t)}{\partial \phi} \quad (4)$$

and $2\pi R$ is the distance traveled by a synchronous particle in one revolution. Let

$$\mathcal{E}_c(\phi, t) \equiv \frac{2\pi R}{V}\mathcal{E}(\phi, t), \quad (5)$$

$$t_c \equiv \sqrt{2\pi h eV f_s f_s'}\, t, \quad (6)$$

and

$$\Gamma \equiv \frac{\dot{w}_s}{eV}. \quad (7)$$

Differentiate (2) with respect to time t and substitute into (3) along with the definitions (5), (6), and (7). Finally

$$\frac{d^2\phi}{dt_c^2} = -\left[\Gamma - \sin\phi\right] - \mathcal{E}_c(\phi, t_c). \quad (8)$$

Equation (8) is the working equation of the computer program.* For each particle F-51[3] integrates Eq. (8) twice using the old momenta and positions of the particles to satisfy the boundary conditions. The evolution of the system with time is then a series of infinitesimal linear transformations.

The space charge fields, $\mathcal{E}_c(\phi, t_c)$, must be normalized to give the proper contribution to the total field. If $U(\phi, t) = g_o \lambda(\phi, t)$,** where $\lambda(\phi, t)$ is the azimuthal charge per unit length and g_o+ is the reciprocal of the capacitance per unit length of a tube of charge of radius a placed halfway between and parallel to two infinite conducting planes separted by a distance G[1], then

$$\frac{\partial U(\phi, t)}{\partial \phi} = g_o \frac{\partial \lambda(\phi, t)}{\partial \phi} \equiv C\int_{-\pi}^{\pi} \lambda(\phi', t)\, K(\phi - \phi')\, d\phi' \quad (9)$$

where the partial differentiation operator is now taken as a convolution with a kernel, $K(\phi - \phi')$, and the constant C is yet to be determined. Equation (9) must be true for all possible distributions of $\lambda(\phi, t)$. In particular, suppose $\lambda(\phi, t) = \beta\phi$ (β is a constant) then,‡ substituting into (9), and evaluating at $\phi = 0$ yields,

$$g_o \beta = -\beta C\int_{-\pi}^{\pi} \phi' K(\phi')\, d\phi' \quad (10)$$

or

$$C = \frac{-g_o}{\int_{-\pi}^{\pi} \phi' K(\phi')\, d\phi'}. \quad (11)$$

Let $\rho_c(\phi, t)$ be the number density of F-51 particles per unit angle ϕ. Then

$$\lambda(\phi, t) = \frac{eN}{nR}\rho_c(\phi, t) \quad (12)$$

where N is the total number of particles in the real system and n is the number of particles used by F-51. Substituting Eqs. (4), (5), (11), and (12) into (9) yields:

*The above discussion is very brief. The references should be consulted for further details.

*For the sake of brevity the computer program will be referred to as F-51 from now on.

**This approximation is appropriate for the long wave length beam modes to be studied.[4]

+$g_o = 1 + 2\ln(2G/\pi a)$. See reference 4 for a derivation of this formula.

‡Many thanks to K. R. Symon for this procedure.

$$\mathcal{E}_c(\phi, t) = \left[\frac{2\pi h e N g_o}{V n R \int_{-\pi}^{\pi} \phi' K(\phi')d\phi'}\right] \int_{-\pi}^{\pi} \rho_c(\phi', t) K(\phi - \phi')d\phi' . \quad (13)$$

The space charge field can also be written as a convolution with an F-51 kernel, $K_c(\phi - \phi')$:

$$\mathcal{E}_c(\phi, t) = \int_{-\pi}^{\pi} \rho_c(\phi', t)\, K_c(\phi - \phi')\, d\phi' . \quad (14)$$

Equating (13) and (14), along with the condition that $K(\phi - \phi') = \alpha K_c(\phi - \phi')$ for α constant, yields the following condition for the integral of the F-51 kernel:

$$\int_{-\pi}^{\pi} \phi' K_c(\phi')\, d\phi' = \frac{2\pi h e N g_o}{V n R} . \quad (15)$$

This expression is used to normalize $K_c(\phi - \phi')$ in F-51. Using a Fourier-analysis method to solve the linearized Maxwell's equations in the tank, Dory shows that the space charge kernel is approximately of the form

$$K(\phi) \propto \frac{\phi}{|\phi|} e^{-\mu\phi}$$

where μ is a large positive constant.[2,1] For computer experiments the kernel is broadened to suppress high harmonic beam modes. Figure 1 shows the F-51 kernel.

II. F-51 Experimental Procedure

The computer experiments were carried out in the following manner. A space charge kernel was computed on the basis of the number of real particles to be used and Eq. (15). Approximately 2000 computer particles were used for each run. This number of particles is small enough so that a run of 200 time steps (2.5 synchrotron periods) takes about 40 minutes of computer time and large enough so that the statistical fluctuations in the azimuthal charge density were small. The initial distribution in $W - \phi$ particle phase space was always of the form

$$\psi(W, \phi, 0) = \sigma U(|W| - |W_I|)\, \rho(\phi, 0) \quad (16)$$

where

$$U(x) = \begin{cases} 1, & x \geq 0 \\ 0, & x < 0 . \end{cases}$$

Equation (16) restricts all particles to lie in a region of phase space bounded by $\pm W_I$ at $t = 0$. Initial energy spreads ΔW_I were taken as $\frac{1}{2}\Delta W_{NM}$, ΔW_{NM}, and $\frac{3}{2}\Delta W_{NM}$. ΔW_{NM} is the energy spread just necessary to stabilize the beam against the "negative-mass" instability. The value of ΔW_{NM} used in the computer experiments was obtained from coasting beam studies where an initial particle distribution was labeled "stable" if there was less than 5 percent change in the particle distribution after a time long compared to a synchrotron period.

Only systems above transition were studied. Two different values for the sine of the stable phase angle were used: $\Gamma = 0.2$ and $\Gamma = 0.75$. For comparison several runs were made to study the RF bucket in the absence of space charge forces (Figs. 2 and 3).

Somewhat arbitrarily, particles whose energies were too large or too small were considered lost to the tank walls and no longer contributed to the space charge field. These maximum and minimum energy values were chosen so that an RF bucket (no space charge forces) with $\Gamma = 0.2$ would just fill one page of computer output (Fig. 2).

The beam was given an initial sinusoidal azimuthal density perturbation so that only a single longitudinal beam mode could be excited.

$$\rho(\phi, 0) = 1 + \epsilon \cos K\phi . \quad (17)$$

The perturbation amplitude was approximately 10 percent ($\epsilon = 0.1$) and K took the values of 2, 5, or 10 ($\rho(\phi, 0)$ appears as the first frame in Figs. 7, 8, 9, 10, 11, and 12 for $K = 5$).

Results

Resumes of the computer experiments are given in Figs. 4, 5, and 6. "Run" is the run number. "K" is the initial perturbation wave number. An "X" under "SC" (space charge) or "RF" indicates that the space charge and/or RF fields were present. "%" is defined as the ratio

$$\frac{\text{final number of particles in phase stable region}}{\text{initial number of particles}} \times 100\% . \quad (18)$$

The final energy spread of the stable phase region ΔW_F is also compared to the initial energy spread ΔW_I.

The $\ddagger$ sign in Fig. 4 indicates runs for which the final phase distribution had a very wide spread in energy and only a narrow spread in phase angle (Figs. 9 and 10). This elliptically shaped distribution occurred only when the initial beam was very unstable. Most of the particles were lost in less than one-half of a synchrotron period. The remaining particles formed one or more cigar-shaped bunches. Due to the space charge forces these elliptic bunches were slowly squeezed in phase angle and stretched in energy

spread. The runs were discontinued after 3-1/2 synchrotron periods. No stable phase region was observed at that time.

Several runs were made with the same initial conditions as the unstable runs mentioned above. The only change that was made was the doubling of the maximum and minimum energies a particle could have before it is considered lost. The particles were captured into a diamond-shaped stable phase region similar to that of Fig. 12. This seems to indicate that the non-stable final phase distributions (Figs. 9 and 10) are the result of not only a strongly unstable initial distribution, but also a limited available space for radial synchrotron oscillations.

Figures 7 and 8 show respectively the results of initially unstable and stable energy spreads for K = 5 and with the RF turned off. In the stable case the initial distribution persisted for five synchrotron periods before high frequency modes began to grow (Fig. 8).

Figures 9 and 10 show the results of runs having the same initial conditions as that of Fig. 7, but with the RF turned on (Γ = 0.2 and 0.75 respectively). Similarly, Figs. 11 and 12 correspond to Fig. 8 with RF (Γ = 0.2 and 0.75 respectively).

In every run where the initial energy spread was greater than or approximately equal to the stable energy spread, the number of particles captured in the stable phase region was greater than the number of particles caught in the corresponding RF bucket with no space charge forces acting. For example (Fig. 5), comparing runs 20080 and 20031 (Γ = 0.2), 85.5 percent were captured with space charge present, and without space charge forces 64.0 percent were captured. In runs 20081 and 20032, 35.8 percent were captured with space charge forces acting as compared to 20.2 percent. Such an increase in the number of particles in the stable phase region is not without its price. In all cases where space charge forces are included, the shape of the stable phase region is not that of the familiar RF bucket (Figs. 2, 3, 11, and 12). The "space charge RF bucket" is more diamond shaped, with less spread in phase angle and with a larger energy spread (compare Figs. 2 and 11; 3 an 12).

There are several features of RF capture that these qualitative results clearly indicate. The space charge effects, per se, compress the beam as it is being trapped in the RF bucket. In the initially stable cases, although the shape of the stable phase region is somewhat different than the usual RF bucket, the areas are approximately the same with more particles in the space charge bucket. In the unstable initial beam cases the final distribution is stable or unstable depending on whether or not there is sufficient room for the radial excursions caused by large amplitude synchrotron oscillations.

References

1. Nielsen, Sessler, Symon; Proc. of Int'l. Conf. on High Energy Accelerators and Instrumentation (CERN, 1959), p. 239.
2. Dory; Nonlinear Azimuthal Space Charge Effects in Particle Accelerators, Ph. D. Thesis, 1962, MURA-654 (unpublished).
3. Dory; Write-Up of MURA 704 Program F-51 Particle Space-Charge Program, MURA-717 (1965, unpublished).
4. Nielsen and Sessler; Rev. Sci. Instr. 30, 80 (1959).

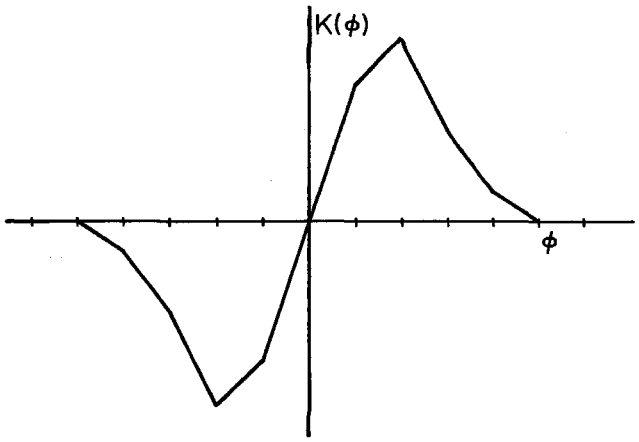

Fig. 1. Space Charge Kernel Used in Computer Program.

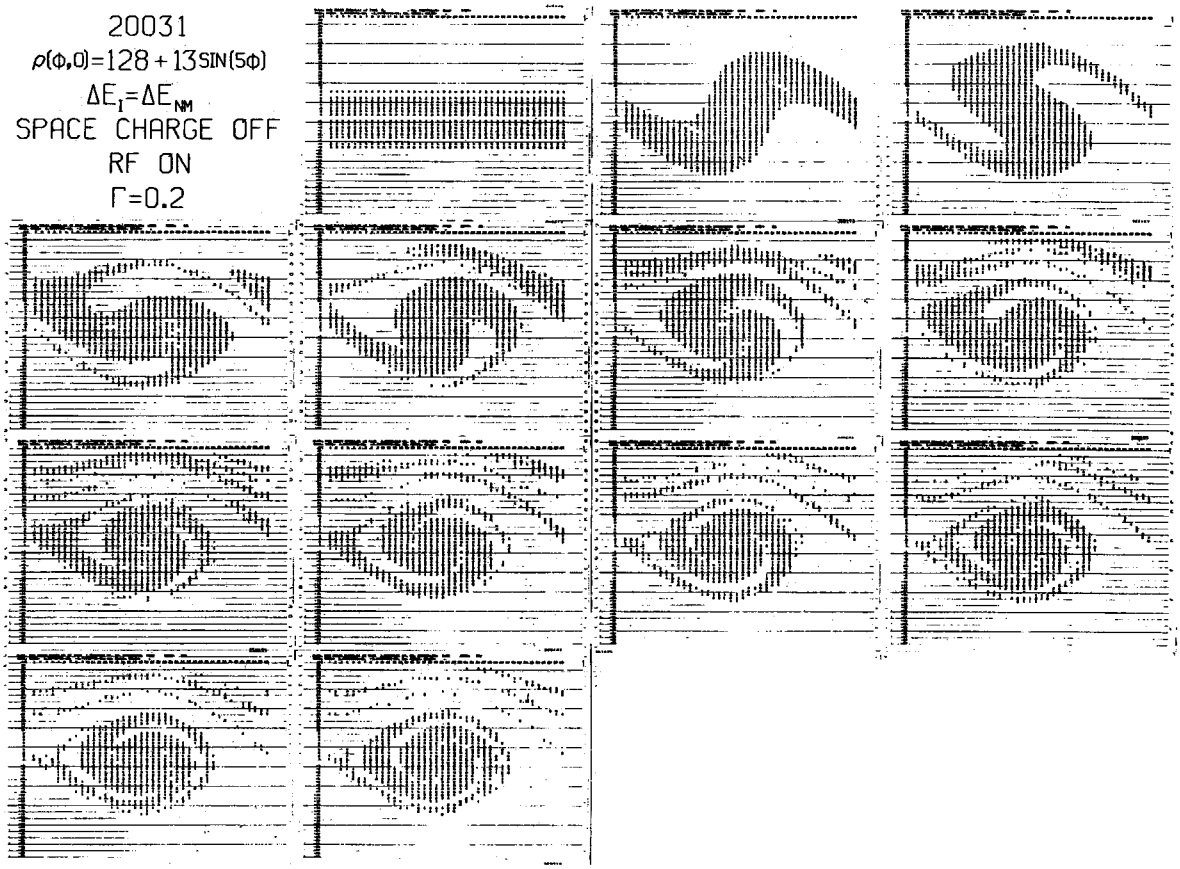

Fig. 2. RF Bucket; Γ = 0.2, No Space Charge.

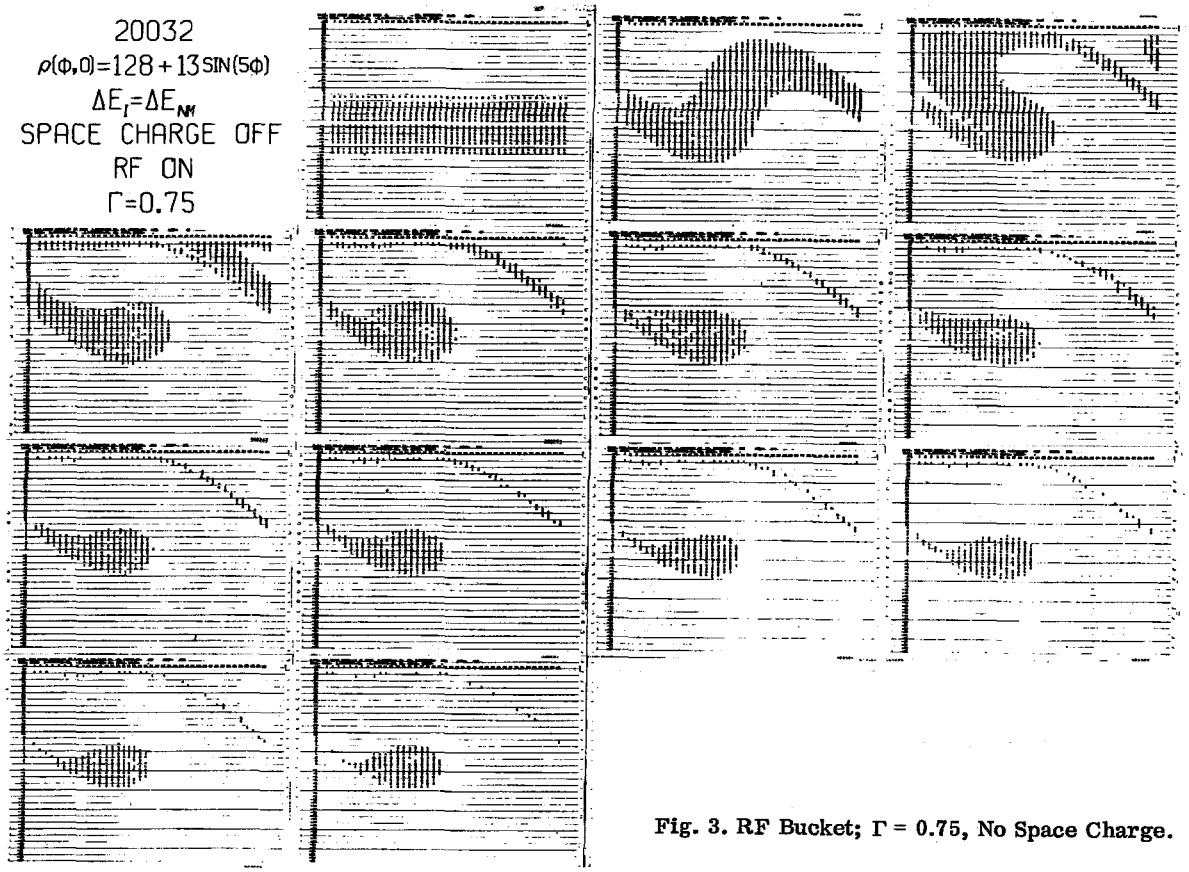

Fig. 3. RF Bucket; Γ = 0.75, No Space Charge.

$\Delta W_I / \Delta W_{NM} = 0.5$

RUN	K	SC	RF	Γ	%	$\Delta W_F/\Delta W_I$
20031			X	0.2	64.2	1.76
20032			X	0.75	20.1	0.43
20103	10	X			95.6	2.31
20104	10	X	X	0.2	32.7	3.00
20105	10	X	X	0.75	43.6	3.13 ‡
20112	2	X			84.4	3.13 ‡
20113	2	X	X	0.2	15.5	2.63
20114	2	X	X	0.75	26.4	3.25‡
20130	5	X			85.4	3.25‡
20131	5	X	X	0.2	17.1	3.25‡
20132	5	X	X	0.75	34.4	3.25‡

Fig. 4. Runs with $\Delta W_I = 0.5\ \Delta W_{NM}$.

$\Delta W_I / \Delta W_{NM} = 1.0$

RUN	K	SC	RF	Γ	%	$\Delta W_F/\Delta W_I$
20031			X	0.2	64.2	1.76
20032			X	0.75	20.1	0.43
20079	10	X			100.0	1.62
20080	10	X	X	0.2	83.1	2.37
20081	10	X	X	0.75	34.8	1.81
20015	2	X			100.0	1.69
20016	2	X	X	0.2	78.3	2.63
20017	2	X	X	0.75	28.0	1.69
20118	5	X			100.0	1.56
20119	5	X	X	0.2	78.5	2.56
20120	5	X	X	0.75	33.3	1.56

Fig. 5. Runs with $\Delta W_I = \Delta W_{NM}$.

$\Delta W_I / \Delta W_{NM} = 1.5$

RUN	K	SC	RF	Γ	%	$\Delta W_F / \Delta W_I$
20031			X	0.2	64.2	1.76
20032			X	0.75	20.1	0.43
20100	10	X			100.0	0.94
20101	10	X	X	0.2	71.0	2.19
20102	10	X	X	0.75	28.1	1.19
20109	2	X			100.0	1.00
20110	2	X	X	0.2	69.5	2.13
20111	2	X	X	0.75	22.2	1.19
20121	5	X			100.0	1.06
20122	5	X	X	0.2	69.2	2.13
20123	5	X	X	0.75	24.7	1.13

Fig. 6. Runs with $\Delta W_I = 1.5\ \Delta W_{NM}$.

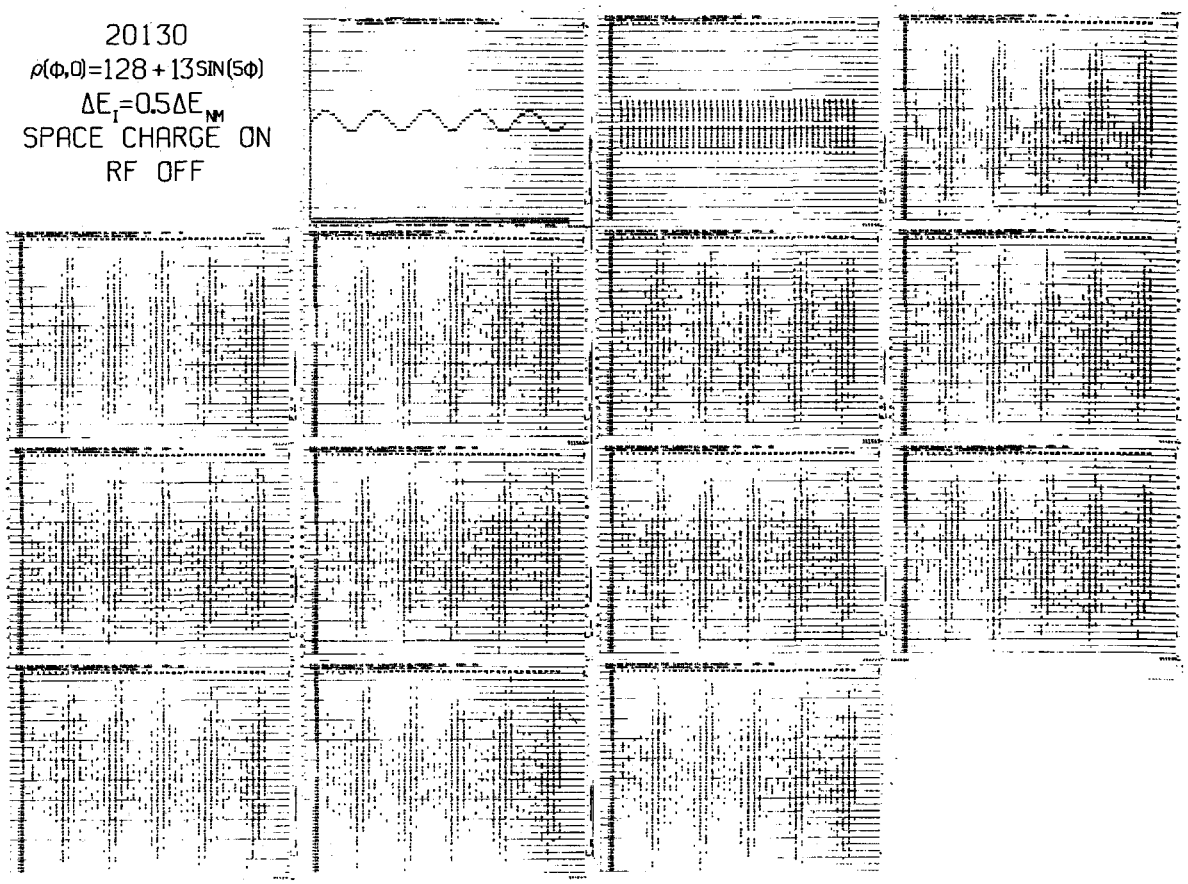

Fig. 7. Growth of Initially Unstable ($0.5\ \Delta W_{NM}$) Beam; No RF.

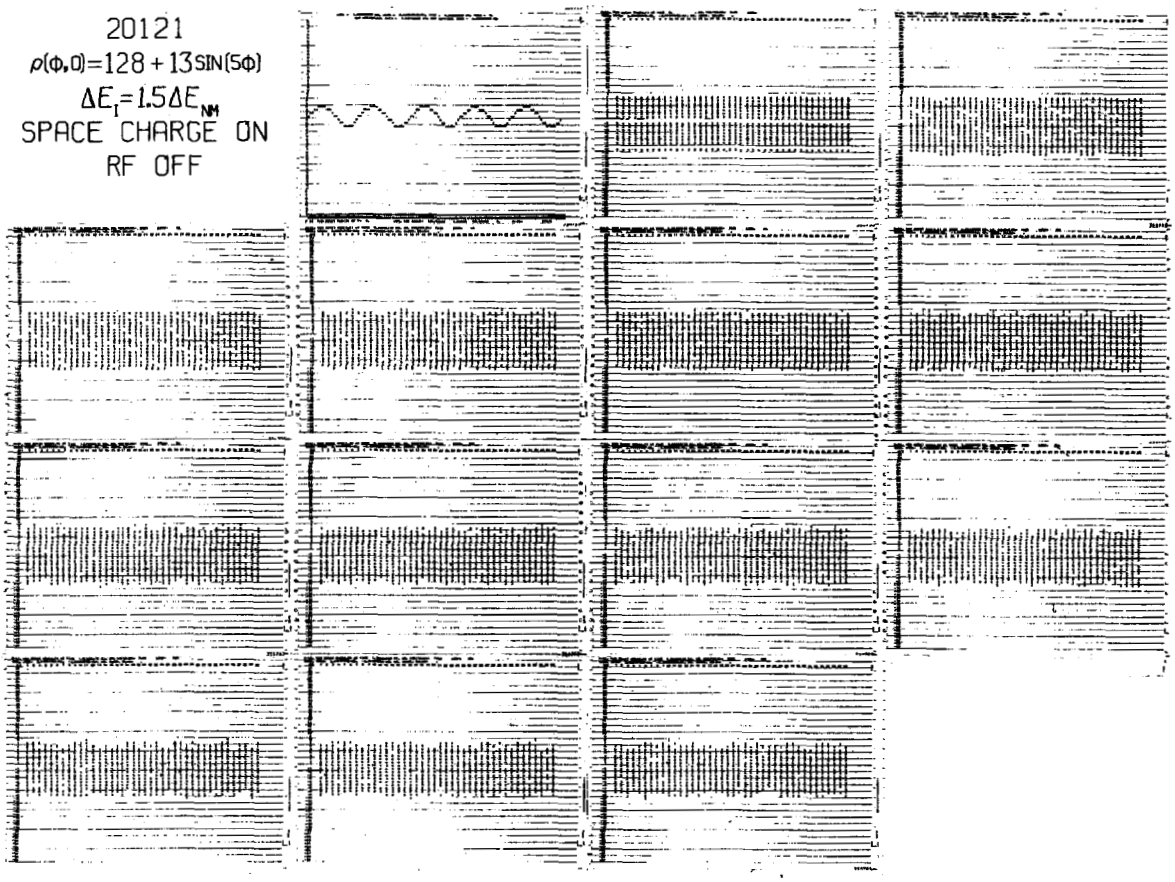

Fig. 8. Growth of Initially Stable (1.5 ΔW_{NM}) Beam; No RF.

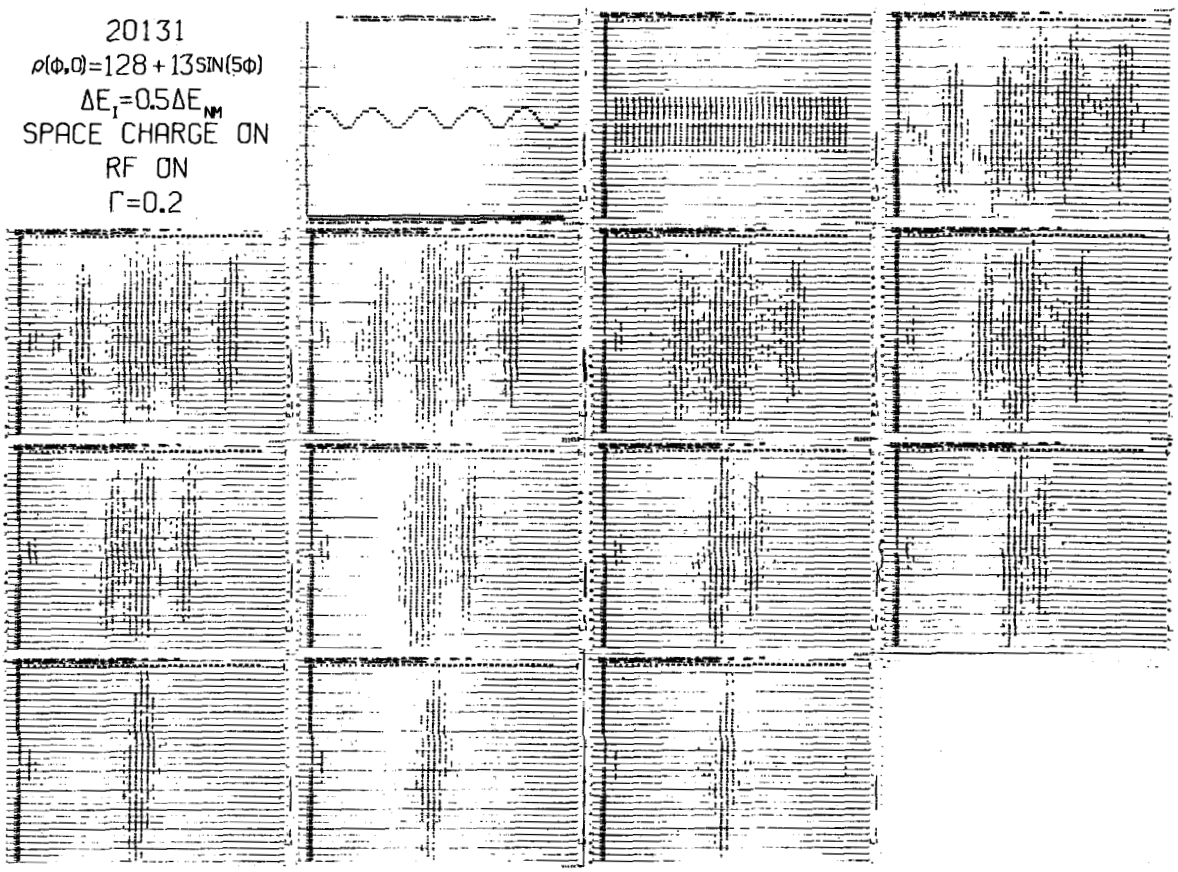

Fig. 9. Space Charge RF Capture; $\Gamma = 0.2$; $\Delta W_I = 0.5\ \Delta W_{NM}$.

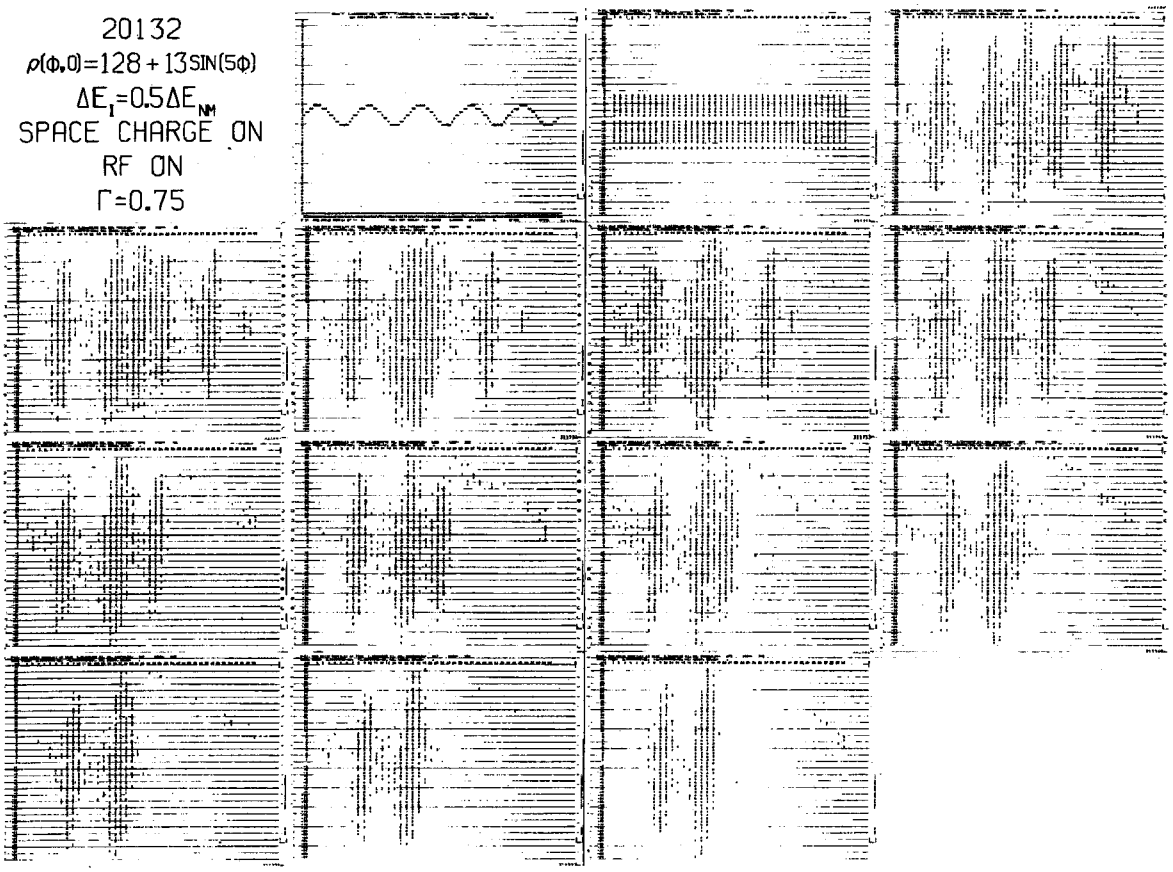

Fig. 10. Space Charge RF Capture; $\Gamma = 0.75$; $\Delta W_I = 0.5\ \Delta W_{NM}$.

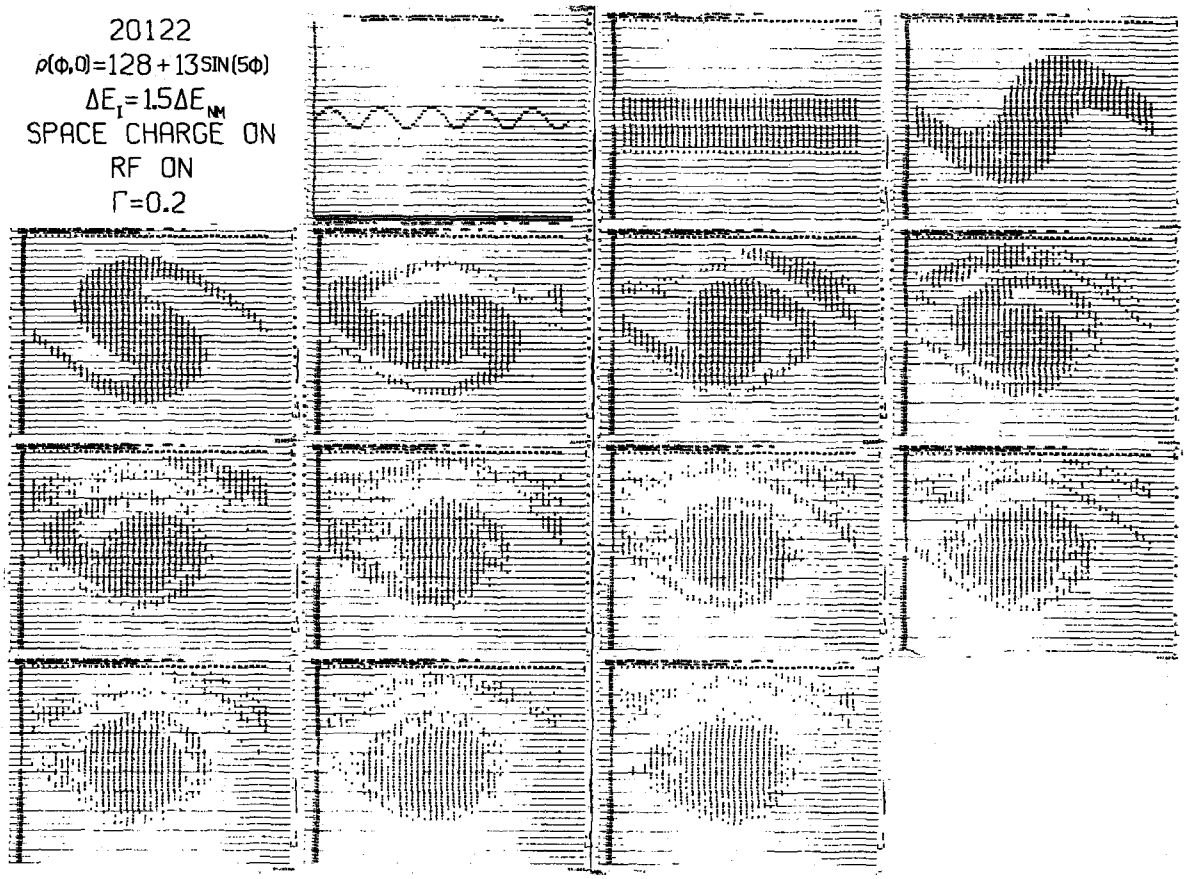

Fig. 11. Space Charge RF Capture; $\Gamma = 0.2$; $\Delta W_I = 1.5\ \Delta W_{NM}$.

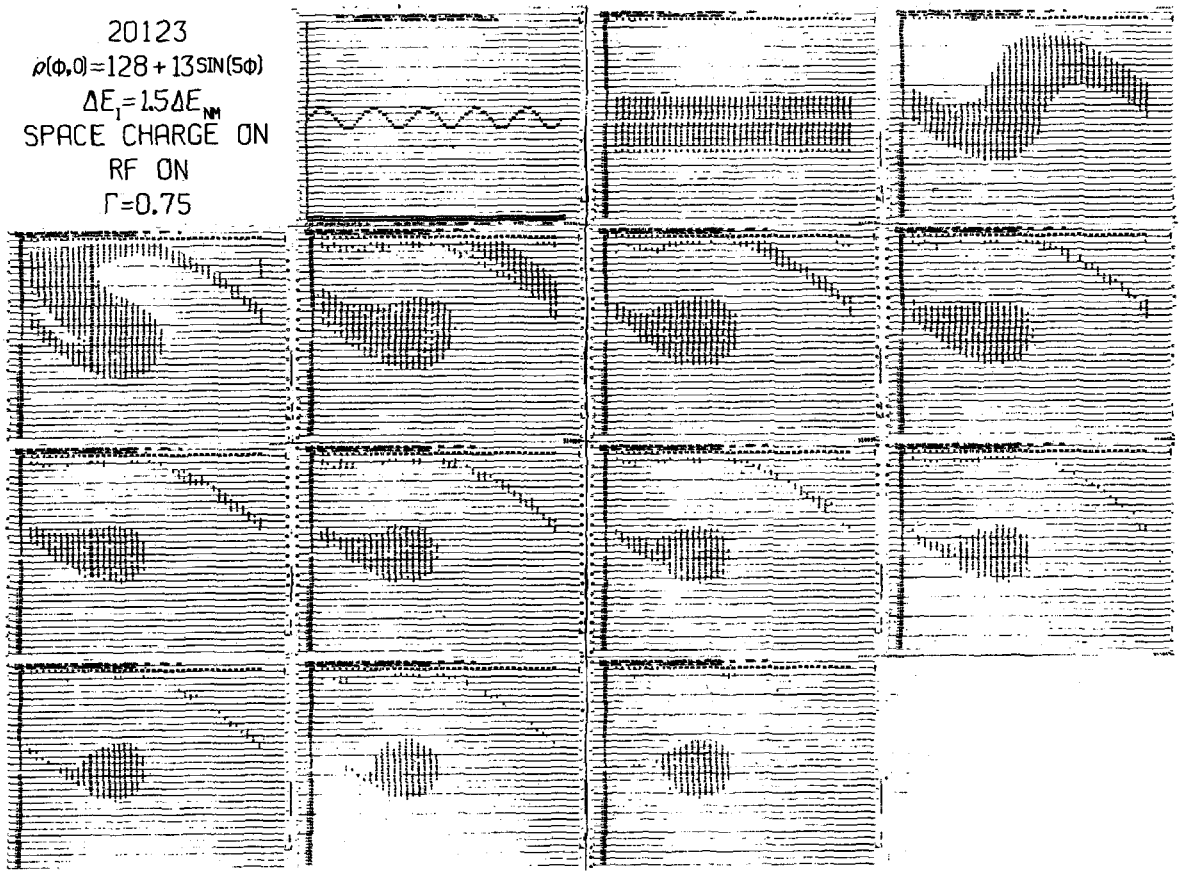

Fig. 12. Space Charge RF Capture; $\Gamma = 0.75$; $\Delta W_I = 1.5\ \Delta W_{NM}$.